J Mater Sci (2017) 52:5324–5332

Rapid preparation of bulk $Al_xYb_{0.25}Co_4Sb_{12}$ (x = 0, 0.1, 0.2, 0.3) skutterudite thermoelectric materials with high figure of merit ZT = 1.36

Mohamed Hamid Elsheikh[1,*], Mohd Faizul Mohd Sabri[2], Suhana Mohd Said[3], Yuzuru Miyazaki[4], H. H. Masjuki[2], Dhafer Abdulameer Shnawah[2], Shuma Naito[4], and Mohamed Bashir Ali Bashir[2]

[1] *Department of Mechanical Engineering, University of Bahri, 13104 Khartoum, Sudan*
[2] *Department of Mechanical Engineering, University of Malaya, 50603 Kuala Lumpur, Malaysia*
[3] *Department of Electrical Engineering, University of Malaya, 50603 Kuala Lumpur, Malaysia*
[4] *Department of Applied Physics, Graduate School of Engineering, Tohoku University, 6-6-05 Aoba, Aramaki, Aoba-ku, Sendai 980-8579, Japan*

Received: 25 August 2016
Accepted: 9 January 2017
Published online: 17 January 2017

ABSTRACT

In this work, a skutterudite-based compound, $Yb_{0.25}Co_4Sb_{12}$, added with Al_x (x = 0, 0.1, 0.2, 0.3) was synthesized with a simple mechanical alloying technique followed by spark plasma sintering. The microstructural properties and thermoelectric properties of the as-sintered samples were investigated. The Al atoms formed AlSb nano-inclusions in the grain boundaries instead of entering the Sb-icosahedral voids, introducing point defects in the matrix lattice. By scattering low-energy electrons, the grain boundaries acted as a potential barrier in simultaneously attaining low electrical resistivity and high Seebeck coefficient. Therefore, $Al_{0.1}Yb_{0.25}Co_4Sb_{12}$ exhibited a high power factor of 4.8×10^{-3} W/m K^2 at 377 °C. AlSb of nanometer length enhanced interfacial phonon scattering, thereby significantly reducing the lattice thermal conductivity of $Al_{0.3}Yb_{0.25}Co_4Sb_{12}$ to 0.6 W/m K at 500 K. The $Al_{0.3}Yb_{0.25}Co_4Sb_{12}$ composite exhibited the highest figure of merit, ZT = 1.36, at 850 K.

Introduction

Thermoelectric materials have attracted extensive research attention because of their environment-friendly applications in waste heat recovery with the Seebeck effect [1–5] and refrigeration with the Peltier effect [6–10]. The efficiency of thermoelectric materials is characterized by the dimensionless figure of merit, $ZT = \alpha^2 T/\rho K$ [11], where α, T, ρ, and K are the Seebeck coefficient, absolute temperature, electrical resistivity, and thermal conductivity, respectively. Developing materials with high electrical conductivity, high Seebeck coefficient, and low thermal conductivity is a significant challenge in

Address correspondence to E-mail: mohdelsheikh84@gmail.com

DOI 10.1007/s10853-017-0772-8

thermoelectric research [12–14]. The phonon-glass-electron crystal (PGEC) concept aims to synthesize the ultimate thermoelectric material that conducts electricity similar to a crystal but insulates heat like a glass [15]. The skutterudite system is a promising material that utilizes the PGEC concept. The skutterudite system relies on crystal "cage-like" structures with loosely bonded filler atoms, mostly from alkaline earth metal and lanthanide elements, to allow simultaneous high electrical and low thermal conductivities.

Numerous filling elements have been explored to enhance the thermoelectric performance of $CoSb_3$-based materials [14, 16–25]. Among these various fillers, Yb is most promising candidate for improving the thermoelectric properties of $CoSb_3$ skutterudite. The $Yb_{0.2}Co_4Sb_{12}$ compound prepared by rapid solidification and spark plasma sintering (SPS) exhibited a maximum ZT of 0.91 at 800 K [20]. The same composition achieved $ZT = 1$ at 823 K when synthesized by encapsulated melting and consolidated by hot pressing [26]. A composite containing $Yb_{0.25}Co_4Sb_{12}$ and well-distributed Yb_2O_3 particles in the grain boundaries attained a maximum ZT of 1.3 at 850 K; the composite was synthesized by in situ reaction method and SPS [27]. A composite of n-type-filled skutterudite $Yb_{0.26}Co_4Sb_{12}$ containing p-type GaSb nano-structured inclusions possessed a ZT value of 1.45 at 850 K [28]. However, $Yb_{0.2}Co_4Sb_{12}$ composite with PbTe inclusions had a relatively low ZT value of 0.78 at 700 K when prepared through simple ball milling and hot pressing [29]. Consequently, introducing nano-structured inclusions into the lattice may reduce the magnitude of thermal conductivity by threefold, hence increasing ZT. However, fabricating high-efficiency skutterudite requires many processes and long production times; as such, minimizing the duration of the fabrication of skutterudite materials remains a challenge.

Selection of appropriate fabrication process and dopant plays key roles in improving the thermoelectric properties of Yb-filled Co_4Sb_{12} skutterudite. Al was added to the ternary skutterudite system $Yb_{0.25}Co_4Sb_{12}$ through ball milling followed by SPS.

Experimental

Elemental powders of Al (320 mesh, >99.99 wt%), Yb (200 mesh, >99.9 wt%), Co (22 mesh, >99.998 wt%), and Sb (200 mesh, >99.99 wt %) were blended at an atomic ratio of x:0.25:4:12 ($x = 0$, 0.1, 0.2, 0.3). Excess amounts of 2 wt% Sb were added to the mixtures to overcome the high volatility of Sb. The mixed powders were subjected to mechanical alloying (MA) with a planetary ball mill (GOKIN Ltd., PLANET) for 10 h. Zirconium oxide vials and balls ($\varphi = 5$ mm) were used. The ball-to-powder weight ratio was maintained at 15:1, and the rotation speed was fixed at 400 rpm. The powders were loaded and unloaded in a glove box filled with an argon atmosphere to avoid contamination and oxidization. Powders pretreated with (MA) were pressed under a vacuum atmosphere by using a SPS system.

Sintering was performed with a heating rate of 100 °C min^{-1} from room temperature to 600 °C. The temperature was then held at 600 °C for 10 min. The sample was left to cool naturally for 2 h. During sintering, the sample was pressed by 36 MPa via a graphite die with an inner diameter of 10 mm.

X-ray diffraction (XRD) analysis was performed to obtain structural information of the disk samples by using a Bruker AXS D8 Advance X-ray diffraction spectrometer with Cu–Kα radiation at a wavelength of 1.5406 Å. Patterns were recorded within the 2θ range of 10° and 90° at a rate of 0.0264 in step width. Imaging at high resolution and real phase structure determination were conducted by the FEI Helios 450HP Dual-Beam FIB-SEM. Seebeck coefficient and electrical resistivity were measured simultaneously on a ZEM-3 (Ulvac-Riko) apparatus. Thermal conductivity was measured on a TC-7000H (Ulvac-Riko) apparatus.

Results and discussion

Microstructure properties

The XRD patterns of the as-sintered samples indicate that the mechanically alloyed powders were highly compacted to a composite polycrystalline skutterudite phase (Fig. 1). The main $Yb_{0.25}Co_4Sb_{12}$ composite contained a small amount of Yb_2O_3 as a secondary phase. The Al-added $Yb_{0.25}Co_4Sb_{12}$ composites contained AlSb as a secondary phase. The crystal structure was refined by JANA2006 [30], and quantitative analysis was conducted by High Score Plus software. The skutterudite phase contributed 99.6 wt% and the Yb_2O_3 secondary phase contributed 0.4 wt% of the $Yb_{0.25}Co_4Sb_{12}$ sample. Therefore, a lattice parameter

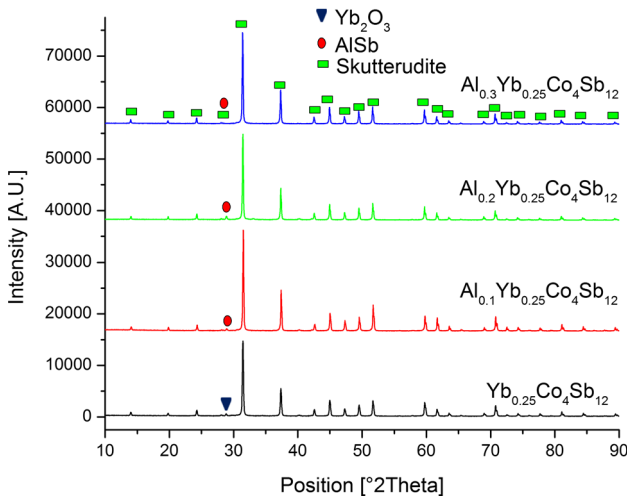

Figure 1 XRD patterns of the as-sintered $Al_xYb_{0.25}Co_4Sb_{12}$ ($x = 0, 0.1, 0.2, 0.3$) composites.

of 9.0394(1) Å was obtained. This result indicates that the Yb atoms did not fill the Co_4Sb_{12} voids. AlSb was present in all Al-added $Yb_{0.25}Co_4Sb_{12}$ ternary skutterudite systems. Additionally, the quantitative analysis of the XRD data indicated that less than 0.2 wt% of AlSb was present in all samples, and the major phase was skutterudite. Therefore, the lattice parameters of $Al_{0.1}Y_{0.25}Co_4Sb_{12}$, $Al_{0.2}Y_{0.25}Co_4Sb_{12}$, and $Al_{0.3}Y_{0.25}Co_4Sb_{12}$ were 9.0470(1), 9.0503(2), and 9.0472(1) Å, respectively.

Figure 2a shows the SEM micrograph of the as-sintered $Yb_{0.25}Co_4Sb_{12}$ sample. The elemental maps indicate that the SPS process on the mechanically alloyed powders did not introduce Yb atoms into the Co_4Sb_{12} voids (Fig. 2b–g). As a result, Yb atoms were found in the grain boundaries beside the O atoms, forming the Yb_2O_3 secondary phase. The SEM micrographs of the as-sintered $Al_{0.1}Y_{0.25}Co_4Sb_{12}$, $Al_{0.2}Y_{0.25}Co_4Sb_{12}$, and $Al_{0.3}Y_{0.25}Co_4Sb_{12}$ samples indicate two types of surface topographies (Figs. 3a, 4a, 5a), respectively. The first topography exhibits aggregated grains in the form of solid islands with very narrow grain boundaries. The second topography exhibits individual grains surrounded by relatively wide grain boundaries.

SEM/EDX verified the presence of an AlSb phase in the grain boundaries of the Al-added skutterudite samples. The microstructure and actual composition of the samples were further investigated with elemental mapping analysis. The elemental maps of the as-sintered $Al_{0.1}Y_{0.25}Co_4Sb_{12}$, $Al_{0.2}Y_{0.25}Co_4Sb_{12}$, and $Al_{0.3}Y_{0.25}Co_4Sb_{12}$ samples clearly illustrate the

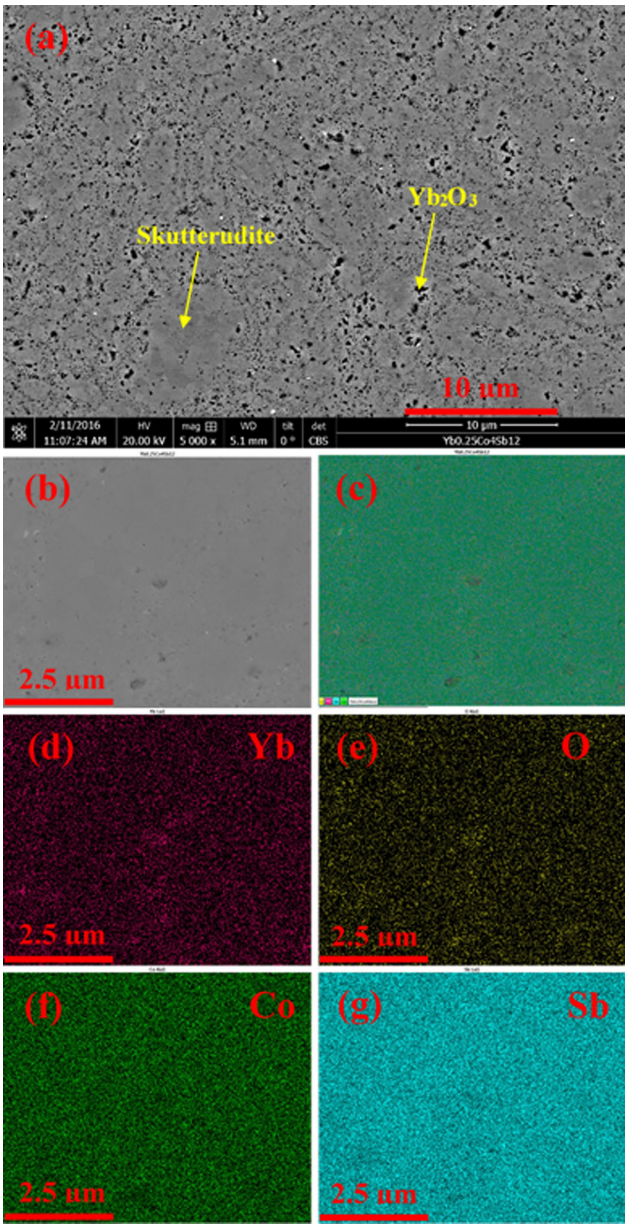

Figure 2 SEM images of $Yb_{0.25}Co_4Sb_{12}$. **a** SEM micrograph of an SPS-compacted sample, **b** SEM/EDX micrograph, and **c** integrated elemental map. The elemental maps of **d** Yb, **e** O, **f** Co, and **g** Sb were extracted from (**b**) with EDX.

distribution of the quaternary system elements (Figs. 3d–g, 4d–g, 5d–g), respectively. Yb, Co, and Sb were systemically distributed on the surfaces of the grains of the as-sintered samples; Al was less present inside the grains but was strongly present in the grain boundaries beside Sb. These results confirm that the skutterudite phase indicated by XRD belongs to the formation of a filled skutterudite phase in grains partially filled by Yb atoms. Moreover, the presence

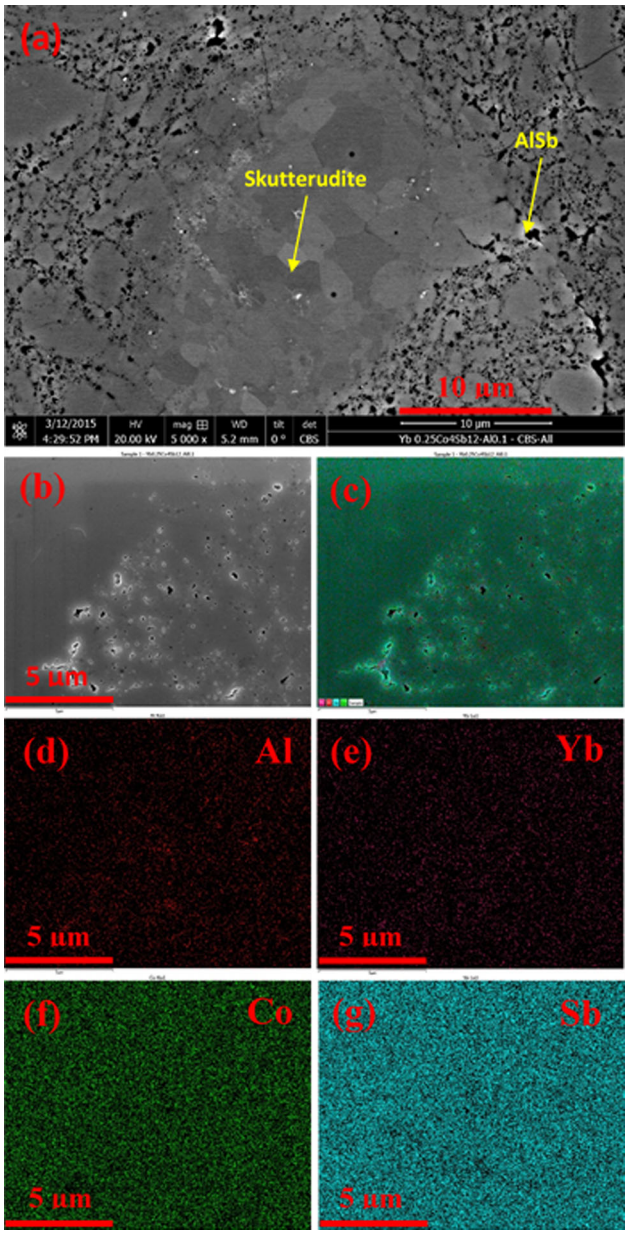

Figure 3 SEM images of $Al_{0.1}Yb_{0.25}Co_4Sb_{12}$. **a** SEM micrograph of an SPS-compacted sample, **b** SEM/EDX micrograph, and **c** integrated elemental map. The elemental maps of **d** Al, **e** Yb, **f** Co, and **g** Sb were extracted from (**b**) with EDX.

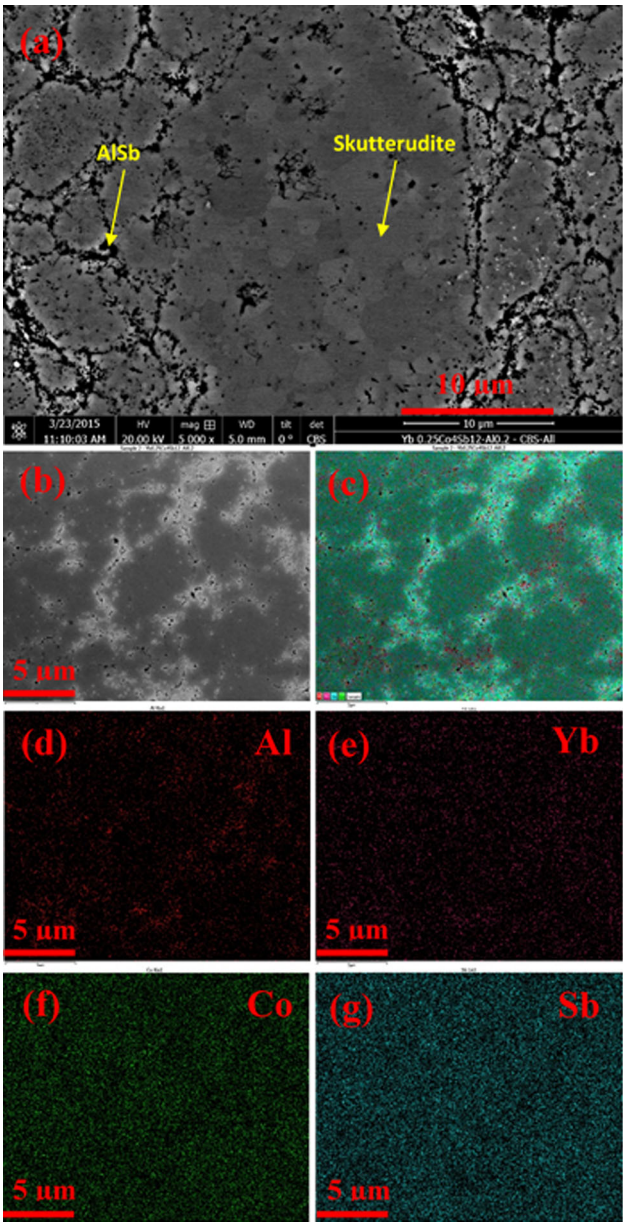

Figure 4 SEM images of $Al_{0.2}Yb_{0.25}Co_4Sb_{12}$. **a** SEM micrograph of an SPS-compacted sample, **b** SEM/EDX micrograph, and **c** integrated elemental map. The elemental maps of **d** Al, **e** Yb, **f** Co, and **g** Sb were extracted from (**b**) with EDX.

of Al beside Sb in the grain boundaries agrees with the AlSb peak indicated in the XRD graph. Inability of Al to fill the skutterudite cage can be explained by the theoretical predictions [31–33] that indicate that the electronegativities (X) of Sb and the filler must satisfy the relation $X_{Sb} - X_{filler} > 0.80$. The Pauling electronegativity of aluminum is 1.61, merely 0.44 smaller than that of antimony, so aluminum should in fact not be able to fill the skutterudite voids.

However, studies of In-doped Co_4Sb_{12} reported that In formed InSb inclusions as a secondary phase instead of entering the Sb-icosahedral voids. Furthermore, these inclusions may potentially reduce lattice thermal conductivity without significantly decreasing the power factor [34]. The $In_{0.4}Co_4Sb_{12}$ composite prepared by Mallik et al. [35] showed a low thermal conductivity of 1.9 W/m K, most likely because a small amount of InSb secondary phase was

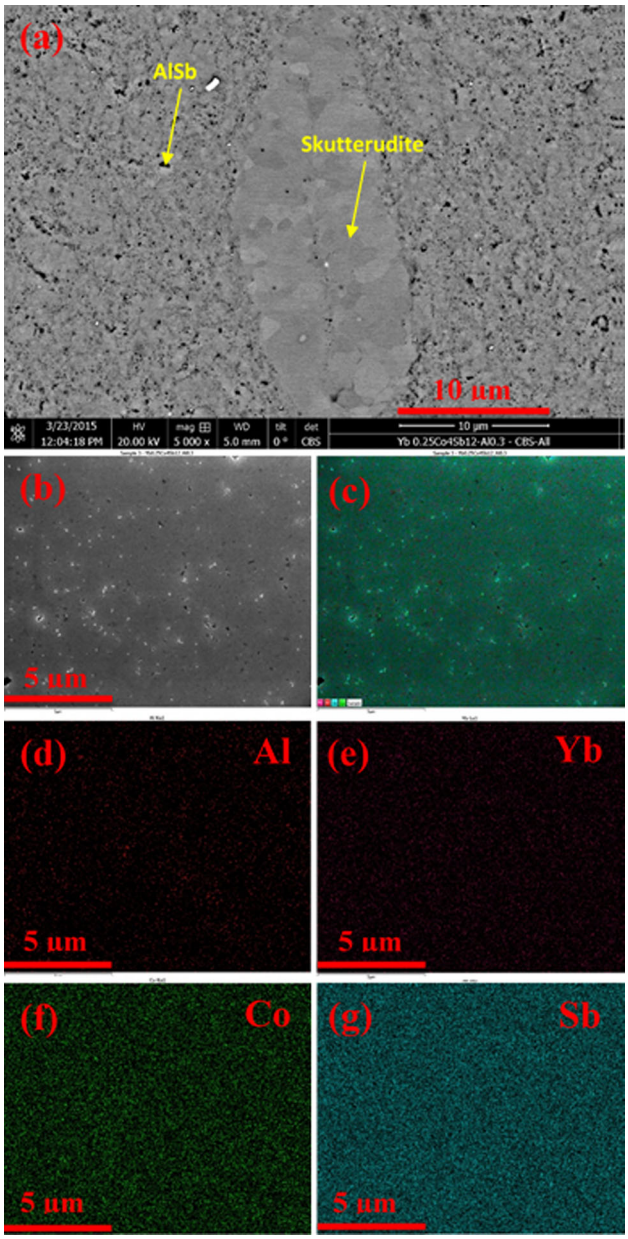

Figure 5 SEM images of $Al_{0.3}Yb_{0.25}Co_4Sb_{12}$. **a** SEM micrograph of an SPS-compacted sample, **b** SEM/EDX micrograph, and **c** integrated elemental map. The elemental maps of **d** Al, **e** Yb, **f** Co, and **g** Sb were extracted from (**b**) with EDX.

finely dispersed at the grain boundaries. Thus, regardless of the non-single-phase morphology, a *ZT* value of 0.96 at 673 K was obtained.

Thermoelectric properties

Figure 6 shows that the electrical resistivity of the $Al_xYb_{0.25}Co_4Sb_{12}$ ($x = 0.1, 0.2, 0.3$) samples is temperature dependent. The $Yb_{0.25}Co_4Sb_{12}$ sample had a

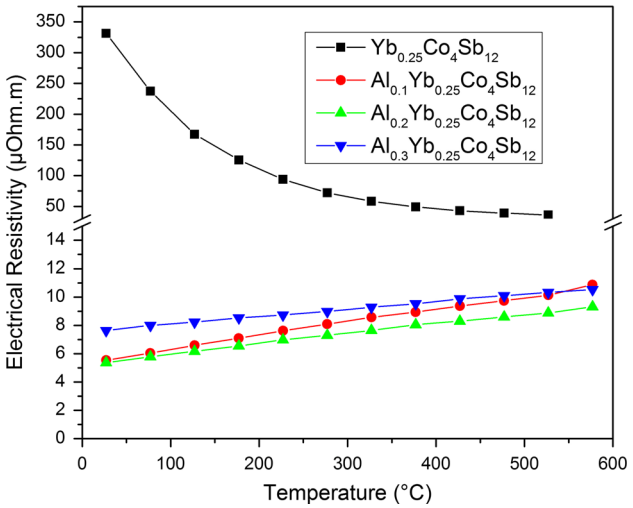

Figure 6 Temperature dependence of the electrical resistivity of $Al_xYb_{0.25}Co_4Sb_{12}$ ($x = 0, 0.1, 0.2, 0.3$) composites.

very high electrical resistivity. However, the Al-added samples demonstrated very low electrical resistivity values over the entire temperature range compared with $Yb_{0.25}Co_4Sb_{12}$. Al-added samples also had very low electrical resistivity values compared with the single-phase $Yb_{0.2}Co_4Sb_{12}$ reported in [20], which had a resistivity of 11.4 μΩm at room temperature. The electrical resistivity of the $Yb_{0.25}Co_4Sb_{12}$ sample decreased as temperature increased, indicating semiconducting behavior. Conversely, the electrical resistivity of the Al-added compositions increased as temperature increased, indicating metal-like behavior over the entire temperature range. This behavior is similar to the behavior of $In_xYb_{0.2}Co_4Sb_{12}$ compositions discussed by Peng et al. [36]. The electrical resistivity range was very narrow for all Al-added samples, i.e., minimum electrical resistivity values of 5.5, 5.3, and 7.6 μΩm at room temperature and maximum electrical resistivity values of 10.9, 9.3, and 10.5 μΩm at 577 °C were recorded for $Al_{0.1}Y_{0.25}Co_4Sb_{12}$, $Al_{0.2}Y_{0.25}Co_4Sb_{12}$, and $Al_{0.3}Y_{0.25}Co_4Sb_{12}$, respectively. Therefore, the average value of electrical resistivity decreased with increasing amounts of AlSb nano-inclusions in the composite. Referring back to the XRD patterns, the $Al_{0.2}Yb_{0.25}Co_4Sb_{12}$ composite had the maximum AlSb content and the minimum electrical resistivity among all composites. This correlation disagrees with previous observations of $Yb_xCo_4Sb_{12}$/yGaSb [28] and $Yb_{0.2}Co_4Sb_{12}$/xPbTe composites [29], in which nano-inclusions increased electrical resistivity.

Figure 7 shows the temperature dependence of the Seebeck coefficients for $Al_xYb_{0.25}Co_4Sb_{12}$ ($x = 0.1, 0.2, 0.3$) samples. The $Yb_{0.25}Co_4Sb_{12}$ sample showed p-type behavior. This behavior resulted from an insufficient number of cations in the Co_4Sb_{12} skutterudite voids. Meanwhile, Al-added samples demonstrated n-type behavior. However, the absolute values of the Seebeck coefficient for all samples showed insignificant differences. The $Yb_{0.25}Co_4Sb_{12}$ sample had a high Seebeck coefficient of 211 μV/K at 127 °C. Subsequently, Seebeck coefficients of 217, 207, and 212 μV/K were obtained for $Al_{0.1}Y_{0.25}Co_4Sb_{12}$, $Al_{0.2}Y_{0.25}Co_4Sb_{12}$, and $Al_{0.3}Y_{0.25}Co_4Sb_{12}$ at 577 °C, respectively. The Seebeck coefficient is strongly associated with the mean carrier energy near the Fermi level [29]. Therefore, high Seebeck coefficients are speculated for all Al-added compositions despite their low electrical resistivity values. High Seebeck coefficients may be attributed to the scattering of low-energy electrons by the grain boundaries potential barrier, the dominant scattering mechanism. Martin et al. [37] proposed that carrier trapping in grain boundaries forms energy barriers that impede the conduction of carriers between grains, essentially filtering charge carriers with energy lower than the barrier height.

Figure 8 illustrates the temperature dependence of the power factors of the $Al_xYb_{0.25}Co_4Sb_{12}$ ($x = 0.1, 0.2, 0.3$) samples. The $Yb_{0.25}Co_4Sb_{12}$ sample had a relatively high Seebeck coefficient; however, it had a very low power factor of 0.44×10^{-3} W/m K^2 at 277 °C as a result of high electrical resistivity. Conversely, the Al-added samples had a very high and stable operating range of power factors. Power factors of 4.9×10^{-3}, 4.7×10^{-3}, and 4.3×10^{-3} W/m K^2, at 377, 327, and 577 °C were obtained for $Al_{0.1}Y_{0.25}Co_4Sb_{12}$, $Al_{0.2}Y_{0.25}Co_4Sb_{12}$, and $Al_{0.3}Y_{0.25}Co_4Sb_{12}$ samples, respectively.

Figure 9 shows the temperature dependence of the thermal conductivity (K) values of $Al_xYb_{0.25}Co_4Sb_{12}$ ($x = 0.1, 0.2, 0.3$) samples. The minimum K for all samples was recorded at room temperature. The temperature dependence of K for The $Yb_{0.25}Co_4Sb_{12}$ indicates a relatively low thermal conductivity of

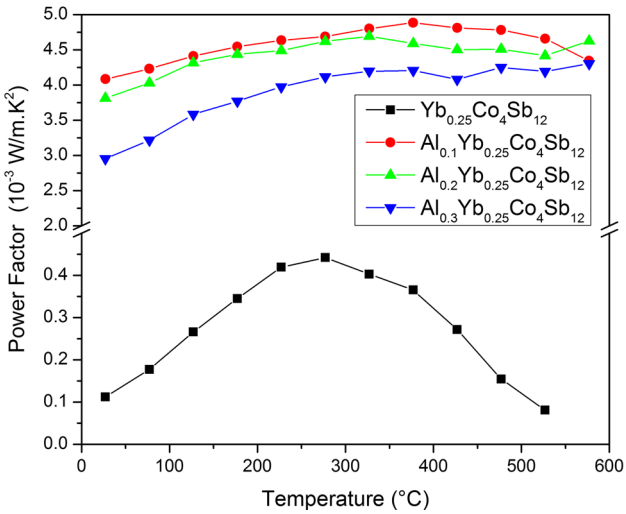

Figure 8 Temperature dependence of the power factor (PF) of $Al_xYb_{0.25}Co_4Sb_{12}$ ($x = 0, 0.1, 0.2, 0.3$) composites.

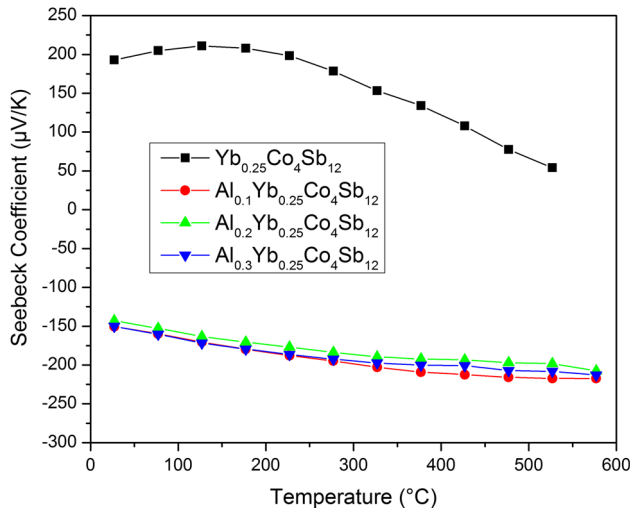

Figure 7 Temperature dependence of the Seebeck coefficient of $Al_xYb_{0.25}Co_4Sb_{12}$ ($x = 0, 0.1, 0.2, 0.3$) composites.

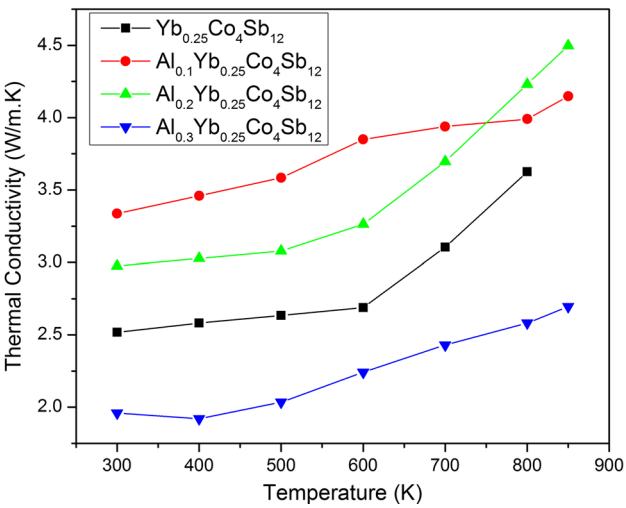

Figure 9 Temperature dependence of the thermal conductivity of $Al_xYb_{0.25}Co_4Sb_{12}$ ($x = 0, 0.1, 0.2, 0.3$) composites.

2.5 W/m K. Yb_2O_3 formation in the grain boundaries increased phonon scattering, hence decreasing the sample's overall thermal conductivity. The $Al_{0.1}Yb_{0.25}Co_4Sb_{12}$ sample had a minimum κ value of 3.3 W/m K. The minimum κ decreased to 3.0 W/m K for the $Al_{0.2}Yb_{0.25}Co_4Sb_{12}$ sample. A significant reduction in κ (1.9 W/m K) was observed in the $Al_{0.3}Yb_{0.25}Co_4Sb_{12}$, sample with high Al content. The gradual increase in the thermal conductivities as a function of temperature for the $Al_{0.1}Yb_{0.25}Co_4Sb_{12}$ and $Al_{0.3}Yb_{0.25}Co_4Sb_{12}$ samples revealed a maximum κ of 4.1 and 2.7 W/m k at 850 K, respectively. The thermal conductivity of the $Al_{0.2}Yb_{0.25}Co_4Sb_{12}$ sample at low temperatures gradually increased to 500 K and rapidly increased after 500 K, resulting in a relatively high thermal conductivity at elevated temperatures.

Figure 10 shows the temperature dependence of the lattice thermal conductivity (κ_L) for $Al_xYb_{0.25}Co_4Sb_{12}$ ($x = 0.1$, 0.2, 0.3) samples. κ_L can be estimated by subtracting the electronic contribution of the Wiedemann–Franz law, $\kappa_e = LT/\rho$, from the total thermal conductivity, where $L = 2.45 \times 10^{-8}$ V^2K^2 is the Lorenz number [22]. Results show that electron thermal conductivity negligibly contributed to the total thermal conductivity of the $Yb_{0.25}Co_4Sb_{12}$ composite. On the contrary, the κ_L of Al-added composites was significantly suppressed compared with the κ_L of the $Yb_{0.25}Co_4Sb_{12}$ composite. Therefore, $Al_{0.1}Y_{0.25}Co_4Sb_{12}$, $Al_{0.2}Y_{0.25}Co_4Sb_{12}$, and $Al_{0.3}Y_{0.25}Co_4Sb_{12}$ had minimum κ_L values of 1.9, 1.3, and 0.6 W/m K at 400, 500, and 500 K, respectively. κ_e contributed more than 60% of the total thermal conductivity in this system. This contribution indicates high electrical transport properties.

The low κ_L of the $Al_{0.3}Yb_{0.25}Co_4Sb_{12}$ sample might be a result of the interaction between the localized modes of the two different dopants with sufficiently different frequencies and the heat-carrying acoustic phonon modes, which might strongly scatter a broader spectrum of heat-carrying phonons. In general, the significant decline in thermal conductivity in the Al-added samples mainly results from the oscillation of the loose Yb cation bond. The anharmonicity of the oscillation of the guest atom can increase phonon scattering. Likewise, the significant drop in thermal conductivity might result from point defects in the lattice microstructure caused by aggregated AlSb nano-inclusions in the grain boundaries and the large area fraction of the grain boundaries [34].

Figure 11 illustrates the dimensionless figure of merit, ZT, for $Al_xYb_{0.25}Co_4Sb_{12}$ ($x = 0.1$, 0.2, 0.3) samples. The $Yb_{0.25}Co_4Sb_{12}$ composite had high electrical resistivity, high Seebeck coefficient, and relatively low lattice thermal conductivity. Therefore, the $Yb_{0.25}Co_4Sb_{12}$ composite also demonstrated a low $ZT = 0.09$ at 600 K. The $Al_xYb_{0.25}Co_4Sb_{12}$ composites containing small amounts of AlSb had low electrical resistivity, high Seebeck coefficient, and low lattice thermal conductivity. These characteristics could be attributed to the phenomenological properties of the

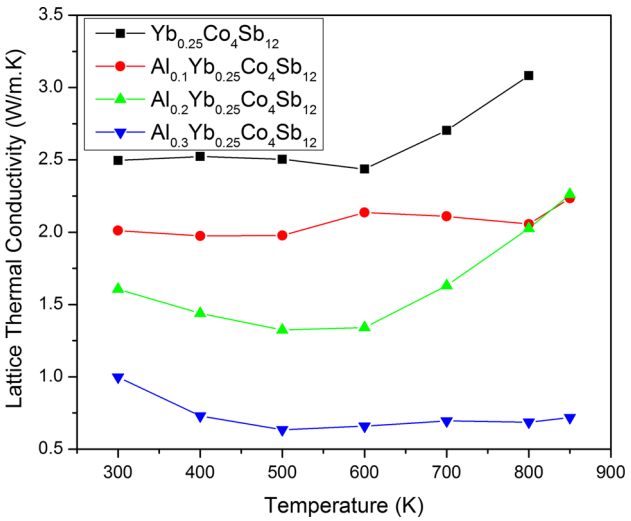

Figure 10 Temperature dependence of the lattice thermal conductivity of $Al_xYb_{0.25}Co_4Sb_{12}$ ($x = 0$, 0.1, 0.2, 0.3) composites.

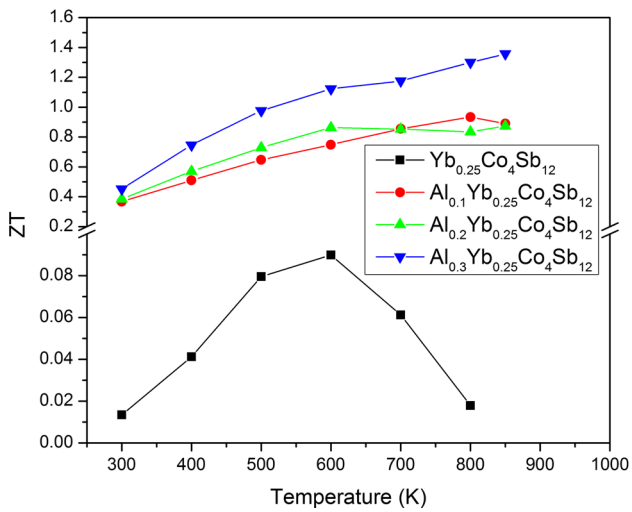

Figure 11 Temperature dependence of the figure of merit, ZT, of $Al_xYb_{0.25}Co_4Sb_{12}$ ($x = 0$, 0.1, 0.2, 0.3) composites.

nanometer-length AlSb scales, including enhanced interfacial phonon scattering and charge carrier filtering. Therefore, high *ZT*s of 0.93, 0.87, and 1.36 at different operating temperatures of 800, 850, and 850 K were obtained for $Al_{0.1}Y_{0.25}Co_4Sb_{12}$, $Al_{0.2}Y_{0.25}Co_4Sb_{12}$, and $Al_{0.3}Y_{0.25}Co_4Sb_{12}$, respectively.

Remarkably, the $Al_xYb_{0.25}Co_4Sb_{12}$ composites containing AlSb nano-inclusions yielded excellent results in terms of a fast fabrication process compared with $Yb_{0.2}Co_4Sb_{12}$ composites containing PbTe inclusions, which showed a lower *ZT* value of 0.78 at 700 K [29]. The main composite of $Yb_{0.2}Co_4Sb_{12}$ was prepared with a lengthy fabrication process. The PbTe inclusions were then introduced into the grain boundaries by the simple process of ball milling and hot pressing. Ballikaya et al. [38] prepared a skutterudite sample with a long fabrication process of melting–annealing followed by SPS. Their synthesized $Yb_{0.2}Ce_{0.15}In_{0.2}Co_4Sb_{12}/Yb_2O_3/Sb$ composite had a high *ZT* of 1.43 at 800 K.

Conclusions

In this work, we demonstrated that producing the $Yb_{0.25}Co_4Sb_{12}$ sample with the simple fabrication process of MA followed by SPS could not introduce Yb atoms into Co_4Sb_{12} skutterudite voids. On the other hand, the same preparation process produced $Al_xYb_{0.25}Co_4Sb_{12}$ ($x = 0.1, 0.2, 0.3$) composites containing small amounts of AlSb and with high thermoelectric properties resulting from the addition of Al. The highest figure of merit, $ZT = 1.36$, was recorded at 850 K for the $Al_{0.3}Yb_{0.25}Co_4Sb_{12}$ composite. The high *ZT* resulted from a significantly decreased lattice thermal conductivity κ_L and a moderately increased electrical conductivity with the addition of 0.3 Al. Therefore, adding Al improves overall TE properties and significantly reduces the duration of the fabrication process. Moreover, the addition of Al to the $Yb_{0.25}Co_4Sb_{12}$ composite induces Yb atoms to fill the Co_4Sb_{12} voids.

Acknowledgements

This work was supported by UMRG (Grant Nos. RP023B-13AET and RP023C/13AET), Science Fund (Grant No. SF020-2013) and FRGS (Grant No. FP022/2014B).

References

[1] Chen W-H, Liao C-Y, Hung C-I, Huang W-L (2012) Experimental study on thermoelectric modules for power generation at various operating conditions. Energy 45:874–881

[2] Gou XL, Yang SW, Xiao H, Ou Q (2013) A dynamic model for thermoelectric generator applied in waste heat recovery. Energy 52:201–209

[3] Jang J-Y, Tsai Y-C (2013) Optimization of thermoelectric generator module spacing and spreader thickness used in a waste heat recovery system. Appl Therm Eng 51:677–689

[4] Lesage FJ, Pagé-Potvin N (2013) Experimental analysis of peak power output of a thermoelectric liquid-to-liquid generator under an increasing electrical load resistance. Energy Convers Manag 66:98–105

[5] Lu H, Wu T, Bai S, Xu K, Huang Y, Gao W, Yin X, Chen L (2013) Experiment on thermal uniformity and pressure drop of exhaust heat exchanger for automotive thermoelectric generator. Energy 54:372–377

[6] Shen LM, Xiao F, Chen HX, Wang SW (2013) Investigation of a novel thermoelectric radiant air-conditioning system. Energy Build 59:123–132

[7] Luo TT, Wang SY, Li H, Tang XF (2013) Low temperature thermoelectric properties of melt spun $Bi_{85}Sb_{15}$ alloys. Intermetallics 32:96–102

[8] Cherkez R (2012) Theoretical studies on the efficiency of air conditioner based on permeable thermoelectric converter. Appl Therm Eng 38:7–13

[9] Chen LG, Meng FK, Sun FR (2012) Effect of heat transfer on the performance of thermoelectric generator-driven thermoelectric refrigerator system. Cryogenics 52:58–65

[10] Meng F, Chen L, Sun F (2011) Performance prediction and irreversibility analysis of a thermoelectric refrigerator with finned heat exchanger. Acta Phys Pol A 120:397–406

[11] Zhu YG, Shen HL, Guan H (2012) Microwave-assisted synthesis and thermoelelectric properties of $CoSb_3$ compounds. J Mater Sci Mater Electron 23:2210–2215

[12] Elsheikh MH, Shnawah DA, Sabri MFM, Said SBM, Hassan MH, Bashir MBA, Mohamad M (2014) A review on thermoelectric renewable energy: principle parameters that affect their performance. Renew Sustain Energy Rev 30:337–355

[13] Bashir MBA, Said SM, Sabri MFM, Shnawah DA, Elsheikh MH (2014) Recent advances on $Mg_2Si_{1-x}Sn_x$ materials for thermoelectric generation. Renew Sustain Energy Rev 37:569–584

[14] Wan S, Huang X, Qiu P, Bai S, Chen L (2015) The effect of short carbon fibers on the thermoelectric and mechanical properties of p-type $CeFe_4Sb_{12}$ skutterudite composites. Mater Design 67:379–384

[15] Glen AS (1995) New materials and performance limits for thermoelectric cooling. CRC handbook of thermoelectrics. CRC Press, Florida

[16] Dyck JS, Chen W, Uher C, Chen L, Tang X, Hirai T (2002) Thermoelectric properties of the n-type filled skutterudite $Ba_{0.3}Co_4Sb_{12}$ doped with Ni. J Appl Phys 91:3698–3705

[17] Song XL, Yang JY, Peng JY, Chen YH, Zhu W, Zhang TJ (2005) Thermoelectric properties of La filled skutterudite prepared by mechanical alloying and hot pressing. J Alloy Compd 399:276–279

[18] Mallik RC, Jung JY, Das VD, Ur SC, Kim IH (2007) Thermoelectric properties of $Sn_zCo_8Sb_{24}$ skutterudites. Solid State Commun 141:233–237

[19] Pei YZ, Bai SQ, Zhao XY, Zhang W, Chen LD (2008) Thermoelectric properties of $Eu_yCo_4Sb_{12}$ filled skutterudites. Solid State Sci 10:1422–1428

[20] Li H, Tang X, Zhang Q (2009) Microstructure and thermoelectric properties of Yb-filled skutterudites prepared by rapid solidification. J Electron Mater 38:1224–1228

[21] Jiang YP, Jia XP, Su TC et al (2010) Thermoelectric properties of $Sm_xCo_4Sb_{12}$ prepared by high pressure and high temperature. J Alloy Compd 493:535–538

[22] Park K-H, Kim I-H (2010) Thermoelectric properties of Ca-filled $CoSb_3$-based skutterudites synthesized by mechanical alloying. J Electron Mater 40:493–498

[23] Deng L, Jia XP, Su TC, Zheng SZ, Guo X, Jie K, Ma HA (2011) The thermoelectric properties of $In_xCo_4Sb_{12}$ alloys prepared by HPHT. Mater Lett 65:2927–2929

[24] Mallik RC, Anbalagan R, Raut KK, Bali A, Royanian E, Bauer E, Rogl G, Rogl P (2013) Thermoelectric properties of Bi-added Co_4Sb_{12} skutterudites. J Phys Condens Matter 25:105701

[25] Zhang Q, Chen C, Kang Y, Li X, Zhang L, Yu D, Tian Y, Xu B (2015) Structural and thermoelectric characterizations of samarium filled $CoSb_3$ skutterudites. Mater Lett 143:41–43

[26] Park KH, Seo WS, Shin DK, Kim IH (2014) Thermoelectric properties of Yb-filled $CoSb_3$ skutterudites. J Korean Phys Soc 65:491–495

[27] Zhao XY, Shi X, Chen LD, Zhang WQ, Bai SQ, Pei YZ, Li XY, Goto T (2006) Synthesis of $Yb_yCo_4Sb_{12}/Yb_2O_3$ composites and their thermoelectric properties. Appl Phys Lett 89:092121

[28] Xiong Z, Chen XH, Huang XY, Bai SQ, Chen LD (2010) High thermoelectric performance of $Yb_{0.26}Co_4Sb_{12}$/yGaSb nanocomposites originating from scattering electrons of low energy. Acta Mater 58:3995–4002

[29] Liu HQ, Zhou G, Sun Q, Gu YJ, Zhao XB (2011) Thermoelectric properties of xPbTe/$Yb_{0.2}Co_4Sb_{12}$ hot-pressed samples. J Inorg Organomet Polym 21:858–861

[30] Petricek V, Dusek M, Palatinus L (2014) Crystallographic computing system JANA2006: general features. Z Kristallogr 229:345–352

[31] Ballikaya S, Wang G, Sun K, Uher C (2011) Thermoelectric properties of triple-filled $Ba_xYb_yIn_zCo_4Sb_{12}$ skutterudites. J Electron Mater 40:570–576

[32] Shi X, Zhang W, Chen LD, Yang J (2005) Filling fraction limit for intrinsic voids in crystals: doping in skutterudites. Phys Rev Lett 95:185503

[33] Uher C (2000) Recent trends in thermoelectric materials research I. In: Tritt TM (ed) Semiconductors and semimetals. Academic Press, San Diego, pp 139–253

[34] Graff J, Zhu S, Holgate T, Peng J, He J, Tritt TM (2011) High-temperature thermoelectric properties of Co_4Sb_{12}-based skutterudites with multiple filler atoms: $Ce_{0.1}In_xYb_y$-Co_4Sb_{12}. J Electron Mater 40:696–701

[35] Mallik RC, Stiewe C, Karpinski G, Hassdorf R, Muller E (2009) Thermoelectric properties of Co_4Sb_{12} skutterudite materials with partial in filling and excess in additions. J Electron Mater 38:1337–1343

[36] Peng JY, He J, Alboni PN, Tritt TM (2009) Synthesis and thermoelectric properties of the double-filled skutterudite $Yb_{0.2}In_{(y)}Co_4Sb_{12}$. J Electron Mater 38:981–984

[37] Martin J, Wang L, Chen L, Nolas GS (2009) Enhanced seebeck coefficient through energy-barrier scattering in PbTe nanocomposites. Phys Rev B 79:115311–115315

[38] Ballikaya S, Uzar N, Yildirim S, Salvador JR, Uher C (2012) High thermoelectric performance of In, Yb, Ce multiple filled $CoSb_3$ based skutterudite compounds. J Solid State Chem 193:31–35